The Astrophysical Journal, 571:501–511, 2002 May 20

RAPID ROTATION OF ULTRA–Li-DEPLETED HALO STARS AND THEIR ASSOCIATION WITH BLUE STRAGGLERS[1]

Sean G. Ryan,[2] Scott G. Gregory,[2] Ulrich Kolb,[2] Timothy C. Beers,[3] and Toshitaka Kajino[4]

Received 2001 December 21; accepted 2002 January 31

ABSTRACT

Observations of 18 halo main-sequence turnoff stars, four of which are extremely deficient in Li, show that three of the Li-poor ones have substantial line broadening. We attribute this to stellar rotation. Despite the great ages of halo stars, for G202-65, BD $+51^\circ1817$, and Wolf 550 we infer $v \sin i = 8.3 \pm 0.4$, 7.6 ± 0.3, and 5.5 ± 0.6 km s^{-1}, respectively. The stated errors are 3 σ. For CD $-31^\circ19466$ we derive a 3 σ upper limit $v \sin i < 2.2$ km s^{-1}. The three rotating stars are known spectroscopic binaries. We explain the high rotation velocities in terms of mass and angular momentum transfer onto the surface of the turnoff star from an initially more massive donor. Estimates of the specific angular momentum of accreted material indicate that quite small transfer masses could have been involved, although the unknown subsequent spin-down of the accretor prevents us from assigning definitive values for each star. The accretor is now seen as an ultra–Li-deficient star whose origin makes it a low-mass counterpart of field blue stragglers. The Li could have been destroyed before or during the mass transfer episode. Such objects must be avoided in studies of the primordial Li abundance and in investigations into the way normal single stars process their initial Li.

Subject headings: stars: abundances — stars: Population II — stars: rotation

1. INTRODUCTION

The lithium content of halo stars near the main-sequence turnoff is of great importance for several reasons. The near constancy of the Li abundances, which are broadly independent of metallicity or effective temperature, led Spite & Spite (1982) to conclude that these were hardly altered from the primordial value. That discovery prompted numerous studies over the ensuing two decades, with the aim of using the inferred primordial abundance as a constraint on the baryon density of the universe, Ω_B (see, e.g., Ryan et al. 2000).

Lithium is also important because it is a sensitive probe of mixing below the stellar surface. Since Li is destroyed in stars at the relatively low temperature of 2.5×10^6 K, it survives in halo main-sequence turnoff stars only in a thin surface layer making up a few percent of the stellar mass. Its destruction in cooler dwarfs (see, e.g., Ryan & Deliyannis 1998 and Cayrel, Lebreton, & Morel 1999) and subgiants (Pilachowski, Sneden, & Booth 1993; Ryan & Deliyannis 1995) provides constraints on stellar structure and evolution models that cannot at present be obtained by any other means. By combining observations with stellar evolutionary models, Pinsonneault et al. (2002) infer that even main-sequence turnoff Population II stars have destroyed $\simeq$0.2 dex of their Li, although Ryan, Norris, & Beers (1999) infer only $<$0.1 dex. The difference in these values depends on (1) the frequency of the few stars with Li abundances significantly lower than the rest, (2) the distribution of their levels of Li deficiency, and (3) whether the deviations are in fact due to the proposed mechanism (rotationally induced mixing) and not some other. These constraints directly impact on the inferred primordial abundance. Small amounts of Li *production* may also be present in the stars that formed more recently from nucleosynthetically enriched material. This can be tracked analogously to the way He production is tracked by dY/dZ.

In stars where some Li is clearly postprimordial, such as where ^{6}Li indicates Galactic production or where elevated ^{7}Li abundances argue strongly for post–big bang production, Li provides important constraints on a range of nucleosynthesis mechanisms and their associated sites. These include cosmic-ray spallation (and fusion) reactions, production in supernovae via the ν-process, and production in stellar sources, such as asymptotic giant branch (AGB) stars, novae, and red giants (see, e.g., Romano et al. 1999, Ryan et al. 2001b, and references therein).

Although the majority of halo main-sequence turnoff stars have almost identical Li abundances, about 7% have very low (thus far undetected) Li abundances at least a factor of 5 below the plateau values expected for their temperatures and metallicities (Spite, Maillard, & Spite 1984; Hobbs & Mathieu 1991; Hobbs, Welty, & Thorburn 1991; Thorburn 1992; Spite et al. 1993; Ryan et al. 2001a). Likewise, a similar fraction of disk stars appear to be anomalously Li-deficient (Lambert, Heath, & Edvardsson 1991; Ryan et al. 2001a). It has been unclear why these small numbers of stars should differ so significantly from the Li-normal stars. Their evolutionary states (Thorburn 1994) and the presence (or lack) of abundance anomalies for other elements (Norris et al. 1997; Ryan, Norris, & Beers 1998) have thus far failed to provide unambiguous evidence of their origin. Citing the common features of Li deficiency and a clustering toward the main-sequence turnoff, Ryan et al. (2001a) suggested a

[1] Based on observations obtained with the University College London echelle spectrograph (UCLES) on the Anglo-Australian Telescope (AAT) and with the Utrecht echelle spectrograph (UES) on the William Herschel Telescope (WHT).

[2] Department of Physics and Astronomy, The Open University, Walton Hall, Milton Keynes, MK7 6AA, UK; s.g.ryan@open.ac.uk, s.gregory@open.ac.uk, u.c.kolb@open.ac.uk.

[3] Department of Physics and Astronomy, Michigan State University, East Lansing, MI 48824-1116; beers@pa.msu.edu.

[4] National Astronomical Observatory, Mitaka, Tokyo, 181-8588 Japan; and Department of Astronomy, University of Tokyo; kajino@ferio.mtk.nao.ac.jp.

common origin with field blue stragglers. They proposed that the same mechanism may produce both classes of objects and that the different names that have been assigned historically ("blue stragglers" and "ultra–Li-deficient stars") depend only on whether they have superturnoff or subturnoff masses. In this paper, a distinction is made between cluster blue stragglers and their field counterparts, because while the former are believed to arise predominantly from collisions, possibly leading to stellar mergers, the latter are more likely the result of mass transfer (Ferraro, Fusi Pecci, & Bellazzini 1995; Mateo et al. 1990; Preston & Sneden 2000).

Ryan et al. (2001b) analyzed the Li abundances of 18 halo main-sequence turnoff stars and found that four of them are ultra–Li-deficient objects. During detailed spectral analysis of other elements (A. Ford et al. 2002, in preparation), we recognized that three of the Li-depleted stars, but none of the Li-normal stars, exhibit unusually broad absorption lines. We believe that this is due to rotational broadening. In this paper we present measurements of the projected rotation velocities and discuss the implications of this discovery for the origin of these systems and their possible link with field blue stragglers.

2. OBSERVATIONS AND MEASUREMENTS

2.1. *Spectra*

The observational program has been described already by Ryan et al. (2001b), so only key details will be repeated here. We had noted previously that studies of the possible dependence of the halo Li abundance on metallicity and effective temperature (a surrogate for mass) were potentially weakened by a nonuniform sampling of these parameters. We set out to improve the situation by observing halo stars with higher-than-average metallicity and effective temperature, since these were the types of stars that had been overlooked. The program stars were selected on the basis of effective temperatures and metallicities estimated from photometric colors and, in some cases, 1 Å resolution blue spectra. Nothing was known about their Li abundances. They were expected to have $6000\ \mathrm{K} \lesssim T_{\mathrm{eff}} \lesssim 6400\ \mathrm{K}$ and $-2 \lesssim [\mathrm{Fe/H}] \lesssim -1$ and hence to provide a supplemental sample of metal-deficient turnoff stars that probed a region of metallicity and temperature space that had been poorly investigated.

Spectra with typical signal-to-noise ratio (S/N) of 50–90 per 0.05 Å pixel were obtained with the University College London echelle spectrograph (UCLES) on the Anglo-Australian Telescope, at a resolving power $\lambda/\Delta\lambda = 43000$ (FWHM = 7.0 km s^{-1}), and with the Utrecht echelle spectrograph (UES) on the William Herschel Telescope, at a resolving power $\lambda/\Delta\lambda = 50000$ (FWHM = 6.0 km s^{-1}). The quoted velocity widths are from measurements of ThAr lines. Importantly, we used observations of ThAr lamps to confirm that the spectrograph resolution was stable through the night.

The spectra included the Li I 6707 Å line and extended to shorter wavelengths, where lines of heavier metals could be observed. Equivalent widths W_{G} were measured by fitting Gaussian profiles using IRAF's SPLOT "kk" facility and are tabulated by A. Ford et al. (2002, in preparation). In the same operation, the fitted Gaussian's FWHM was also recorded.

2.2. *Line Profiles*

The measurements of Fe I lines were scrutinized for potential blends by examining the dependence of FWHM on W_{G}. The expectation was that lines formed from the blending of two or more components would have unusually large Gaussian widths for their equivalent widths. However, comparison of the data for the various stars showed that the Li-deficient objects had systematically broader line profiles than the normal stars.

Figure 1 shows the FWHM of the Fe I lines of Li-normal stars as a function of the measured equivalent width. Lines with equivalent widths in the range $30\ \mathrm{mÅ} \lesssim W_{\mathrm{G}} \lesssim 120\ \mathrm{mÅ}$ exhibit a slight increase of FWHM from 9 to 10 km s^{-1} as the spectral lines strengthen and their Gaussian cores saturate. The intrinsic FWHM of the lines due to natural, thermal, microturbulent, and collisional broadening is only 3–4 km s^{-1}, so the observed value is dominated by the finite spectral resolution of the adopted spectrograph setup (6.0 and 7.0 km s^{-1} for UES and UCLES, respectively), plus a contribution from macroturbulence, which we discuss below. Note that the UCLES and UES data are just distinguishable, consistent with the slightly better spectral resolution employed with UES. Lines weaker than 30 mÅ are considerably affected by noise, such that the diagram fans out to higher and lower FWHM.

For the weakest lines, FWHM should depend only weakly on W_{G}, but it is likely that a selection bias depopulates the top left of the diagram. Lines whose errors conspire to produce shallow lines would give rise to small equivalent widths and large FWHM, but these are more likely to be overlooked in the measurement process. Lines with the same equivalent width but smaller FWHM will be deeper and more likely to be measured. There is some evidence of

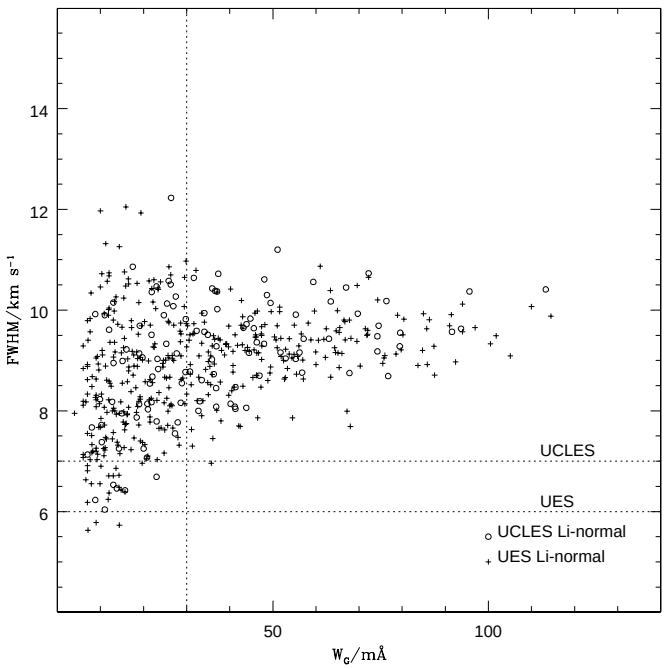

FIG. 1.—Gaussian fit parameters for Fe I lines in Li-normal stars. *Plus signs*: UES data for Li-normal stars. *Circles*: UCLES data for Li-normal stars. The vertical dashed line at 30 mÅ indicates a low-W_{G} cutoff, below which noise dominates and we neglect the measurements. The horizontal dashed lines show the instrumental FWHM of the two spectrograph configurations.

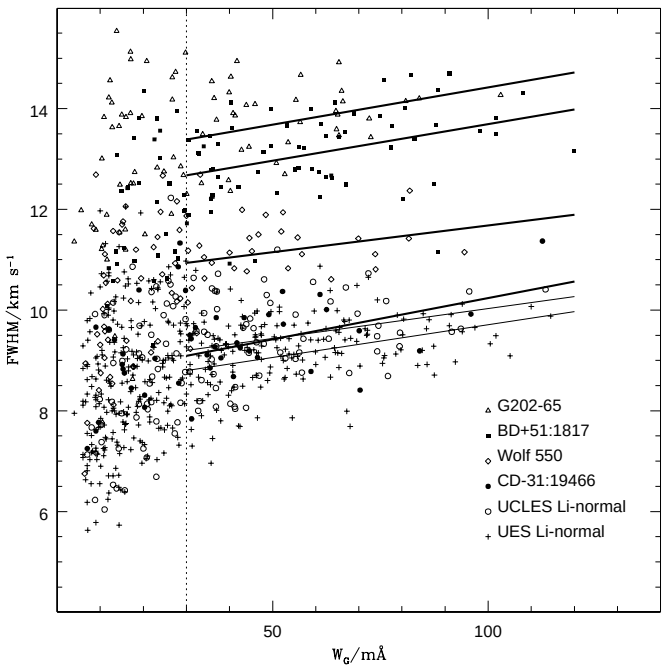

FIG. 2.—Gaussian fit parameters for Fe I lines in all stars. *Plus signs*: UES data for Li-normal stars. *Open circles*: UCLES data for Li-normal stars. *Other symbols*: Li-poor stars. *Heavy lines*: Least-squares fits to lines with $W > 30$ mÅ in (*from top to bottom*) G202-65, BD +51°1817, Wolf 550, and CD −31°19466. *Light lines*: Least-squares fits to lines with $W_G > 30$ mÅ in Li-normal stars observed with UCLES (*upper*) and UES (*lower*).

such a bias in the figure. Because of this and the increasing relative errors in the weakest lines, we do not rely on the profile measurements of lines weaker than 30 mÅ in the subsequent analysis.

Figure 2 extends Figure 1 with the inclusion of the four ultra–Li-poor stars. CD −31°19466 is indistinguishable from Li-normal stars similarly observed with UCLES, but the other three, all observed with UES, have broader lines than Li-normal UES stars. The figure also shows linear least-squares fits to the subset of lines with equivalent widths $W_G > 30$ mÅ. The fits are listed in Table 1. Clearly an additional broadening mechanism is at work in three of the stars. The fact that three out of four Li-poor stars show this broadening, whereas none of the 16 Li-normal stars show the effect, strongly suggests that the broadening is related to the extreme Li deficiency of these objects.

3. ANALYSIS

3.1. *Line-broadening Mechanisms*

In this subsection, we consider mechanisms that might be capable of producing the excess broadening in the Li-poor stars. If it was produced by a Gaussian mechanism, then the additional broadening required, FWHM_+, could be estimated as the difference (in quadrature) between the Gaussian FWHM measured for the Li-depleted stars and that for the Li-normal stars. By evaluating the difference in the least-squares fits at $W_G = 50$ mÅ, we obtain the broadening velocities listed in Table 1.

One Gaussian broadening mechanism is microturbulence, but we note at the outset that extreme values of microturbulence are not responsible. Quite apart from the uncommonly large velocities that would be required, the abundance analysis (A. Ford et al. 2002, in preparation) resulted in normal microturbulent velocities being derived for these stars, $\xi \simeq 1$ km s^{-1}.

An alternative mechanism is macroturbulence. The radial-tangential assumption for macroturbulence produces a non-Gaussian broadening function having a sharp core and nonzero wings that are less pronounced than those of a Gaussian (see, e.g., Gray 1992). Measurements of macroturbulence have rarely been made in halo stars, since the values are so low that very high resolving powers are essential. However, they have been measured in analyses of the ^{6}Li/^{7}Li isotope ratio in a few stars. In their analysis of HD 76932, Nissen, Lambert, & Smith (1994) used a one-dimensional model atmosphere to derive a radial-tangential macroturbulent component with FWHM = 4.7 km s^{-1}. For a larger sample of halo turnoff stars, Smith, Lambert, & Nissen (1998) derived Gaussian macroturbulent values, FWHM_Γ, in the range 4.4–6.1 km s^{-1}. In their analysis of G271-162, Nissen et al. (2000) derived two measures separately for one-dimensional and three-dimensional model atmospheres. The former required $\mathrm{FWHM}_\Gamma = 5.9 \pm 0.1$ km s^{-1}. In the three-dimensional hydrodynamical model, the microturbulent and macroturbulent velocity fields are inherent in the model, and only a small rotational component ($v \sin i = 2.9 \pm 0.1$ km s^{-1}) needed to be added.

The observed FWHM values for the Li-normal stars could be explained by macroturbulence of the magnitude found by Smith et al. (1998). For example, if lines with $W_G = 50$ mÅ have intrinsic widths $\mathrm{FWHM}_{\mathrm{int}} = 3.5$ km s^{-1}, experience Gaussian macroturbulence with $\mathrm{FWHM}_\Gamma = 6.0$ km s^{-1}, and encounter Gaussian instrumental profiles with $\mathrm{FWHM}_{\mathrm{inst}} = 6.0$ and 7.0 km s^{-1}, then we would expect to observe FWHM = 9.2 and 9.9 km s^{-1}, respectively. This is consistent with the values observed for the Li-normal stars. In contrast, very large FWHM_Γ-values would be required to match those for the Li-poor ones. Li-poor stars with intrinsic widths $\mathrm{FWHM}_{\mathrm{int}} = 3.5$ km s^{-1}, observed on UES at an instrumental $\mathrm{FWHM}_{\mathrm{inst}} = 6.0$ km s^{-1}, would require FWHM_Γ of 8.5 km s^{-1} to reach an observed FWHM of 11.0 km s^{-1} and $\mathrm{FWHM}_\Gamma = 11.6$ km s^{-1} to reach an observed FWHM of 13.5 km s^{-1}. Although these values are large compared with ones found previously, we should bear in mind that Li-depleted stars are *not* normal, so we should remain open to the possibility that they may have unusually turbulent atmospheres. It would be valuable to obtain higher S/N spectra to test whether the line profiles could be fitted by macroturbulence. If they could, the turbulence may be related to a mixing process that led to the destruction of the surface Li. That is, if large-scale motions in the stellar atmosphere have carried surface Li to depths great enough to destroy it, then perhaps we are seeing that motion directly. It would remain, however, to identify the mechanism responsible for driving that motion and how it might be sustained to the present in halo stars with ages ≃12–14 Gyr.

Another alternative, which we consider more likely, is that the broadening is due to rotation. Normal halo dwarfs do not rotate perceptibly. There are few measurements of rotation in halo main-sequence stars, again because it is generally below the level of detectability at the resolving power $R < 40,000$ at which these stars are typically observed. It is for this reason that we are forced to use the 14 Li-normal

TABLE 1

STELLAR PARAMETERS

Object (1)	Instrument (2)	Least-squares Fit FWHM[a] (km s^{-1}) (3)	rms (km s^{-1}) (4)	FWHM$_+$ (km s^{-1}) (5)	$v \sin i \pm 3\sigma$ (km s^{-1}) (6)	$T_{\rm eff}$ Photometric (7)	[Fe/H] Old (8)	[Fe/H] New (9)	$T_{\rm eff}$ χ (10)	[Fe/H] χ (11)	$P_{\rm orb}$[b] (days) (12)	e[b] (13)	$M_2 \sin i$[b] ($M_\odot$) (14)	$i_{\rm NS}$[c] (deg) (15)
Li-normal	UCLES	$0.0145W_{\rm G} + 8.78$	0.72	...	...	...	...	...	...	...	...	...	...	...
CD $-31°19466$.....	UCLES	$0.0157W_{\rm G} + 8.63$	0.61	0.0	<2.2	5986	-1.89	-1.66	6190	-1.50	...	...	...	...
Li-normal	UES	$0.0126W_{\rm G} + 8.55$	0.64	...	...	...	...	...	...	...	...	...	...	...
Wolf 550[d].....	UES	$0.0106W_{\rm G} + 10.62$	0.70	6.3	5.5 ± 0.6	6269	-1.66	-1.56	6570	-1.32	688	0.29 ± 0.04	0.26	10
BD $+51°1817$.....	UES	$0.0145W_{\rm G} + 12.24$	0.78	9.2	7.6 ± 0.3	6345	-1.10	-0.88	6920	-0.48	517	0.043 ± 0.028	0.35	14
G202-65.....	UES	$0.0148W_{\rm G} + 12.94$	0.70	10.1	8.3 ± 0.4	6390	-1.50	-1.32	6900	-0.93	167.54	0.15 ± 0.02	0.50	31

[a] $W_{\rm G}$ in units of milliangstroms.

[b] Carney et al. 2001.

[c] Inclination $i_{\rm NS}$ *if* the companion is a neutron star with mass 1.4 $M_\odot$.

[d] G66-30.

stars in our sample as the nonrotating reference stars. However, Smith et al. (1998) do provide guideline measurements for nine halo stars, for which they find $v \sin i \leq 2$–3 km s^{-1}. The reason for the low rotation of halo dwarfs is that they have presumably spun down by magnetic breaking over their long lifetimes. However, the Li-depleted stars clearly are peculiar, and it is quite possible that three of them have high rotation velocities.

A rotational broadening profile is non-Gaussian, so the rotation velocity cannot be derived as easily as the Gaussian broadening velocity FWHM_+ above, but nevertheless, it must be of the same order of magnitude. Rotation estimates are made below. We defer our discussion of the implications of measured rotation velocities to § 4 and instead continue here by explaining how velocity measurements were made from the broadened spectral lines.

3.2. *Rotational Broadening Measurements*

Gray (1992) derives an analytic broadening function for the case where rotational broadening dominates a line profile. Gray suggests a value $v \sin i > 15$ km s^{-1} for this condition to be satisfied. Although for our stars we infer slower rotation than this, $\simeq$5.5–8.3 km s^{-1}, spectrum synthesis suggests that the nonrotating intrinsic line width, $\mathrm{FWHM}_{\mathrm{int}}$, is only 3–4 km s^{-1}, so rotation apparently does dominate. It is possible that our derived rotation velocities are slightly in error because of this simplification, but the resulting (small) discrepancy should not affect our conclusions.

The broadening profile due to stellar rotation has two components, one elliptical and one parabolic. In contrast to Gaussian, Lorentzian, Voigt, and macroturbulent profiles, the rotational profile has no wings beyond $\Delta\lambda = \pm\lambda(v \sin i)/c$, so the resulting profile is a sharp U shape, scaled in wavelength by the projected equatorial rotation velocity $v \sin i$. The relative contribution of the two parts of the profile depends on the limb darkening of the star, which enters Gray's formula via a parameter η, which we set equal to 0.6. The model assumes no differential rotation of the stellar surface layers.

The rotation velocities of the Li-deficient stars were calculated as follows. Synthetic spectra were computed using code that originated with Cottrell & Norris (1978). The stellar atmosphere parameters and models were the same as adopted by Ryan et al. (2001b), and the line list was the same set of Fe I lines measured by A. Ford et al. (2002, in preparation) and used in Figure 2.

The synthetic spectra were first broadened by Gaussian profiles intended to match the instrumental and macroturbulent broadening, and then the spectral lines were measured using the same IRAF Gaussian-fitting routine as was used for the observed spectra. In this way, FWHM- and W_{G}-values were obtained for the synthetic spectra that could be compared with those from the observations.

The FWHM of the synthesized lines is not uniquely a function of W_{G}, but also depends slightly on the lower excitation potential χ_{low} of the transition. This dependence reflects the greater depths at which lines of higher excitation potential form (see, e.g., Figs. 13.2 and 13.3 of Gray 1992). Because of this depth dependence, two lines having the same equivalent width W but different excitation potentials will have different profiles and hence different values of W_{G} (which is the Gaussian approximation to the equivalent width W). It is for these reasons that it is important to use the same spectral lines in the synthetic spectra as in the observations.[5] Note that the range in FWHM brought about by the χ_{low} dependence is less than the observed spread, which is to say that random errors in line measurements dominate the observed spread and could be reduced with higher S/N data.

The Gaussian broadening was varied until the run of FWHM versus W_{G} matched that seen in Figure 2 for the Li-normal stars. Specifically, a least-squares fit was performed on the measurements of the synthesized lines, just as had been done for the real data, and the two least-squares fits were compared at $W = 50$ mÅ. This choice of line strength was made because such lines are strong enough to avoid much of the noise that affects weaker lines in the observed spectra and are central enough in the distributions of both W_{G} and FWHM to avoid being grossly affected by outlying data.

The Gaussian FWHM required to achieve this match was 8.1 ± 0.1 km s^{-1} for the UCLES spectrum and 7.8 ± 0.1 km s^{-1} for the UES spectrum. Subtracting (in quadrature) the known underlying instrumental values implies average macroturbulent values $\mathrm{FWHM}_\Gamma = 4.1$ km s^{-1} for the UCLES sample and 5.0 km s^{-1} for the UES sample. The stated 1 σ uncertainties reflect the standard error in the mean of the observed FWHM values, based on the scatter about the least-squares fit. These instrumental and macroturbulent components supplement the natural, thermal, collisional, and microturbulent broadening incorporated in the synthesis.

Once the line broadening of the Li-normal stars was reproduced, the Gaussian components were frozen, and the rotational broadening was increased from zero to determine what value of $v \sin i$ was required to reproduce the run of FWHM versus W_{G} in the Li-depleted stars. The set of lines synthesized was tuned from star to star to match the list of lines actually observed. The synthesized lines were then measured using the same Gaussian-fitting routine as for the observations, and a least-squares fit was made to the run of FWHM versus W_{G} for the lines with $W_{\mathrm{G}} > 30$ mÅ. Figure 3 shows the least-squares fits for the synthetic spectra, along with the observational data for the Li-poor stars. The match between the observed and synthesized fits was again made at $W_{\mathrm{G}} = 50$ mÅ. The derived $v \sin i$ velocities are given in column (6) of Table 1. The tabulated uncertainty is the change in $v \sin i$ required to alter FWHM (at $W_{\mathrm{G}} = 50$ mÅ) by 3 times the value $\mathrm{rms}/n^{1/2}$, where n is the number of spectral lines in the least-squares fit and rms is the scatter about the fit. Similarly, the upper limit on $v \sin i$ for CD $-31°19466$ is the change in $v \sin i$ required to alter FWHM (at $W_{\mathrm{G}} = 50$ mÅ) by 3 times the value $\mathrm{rms}/n^{1/2}$.

We note for completeness that the run of FWHM versus W_{G} for the synthetic spectra was slightly steeper than for the observed lines. The origin of this mismatch could be a combination of the effects of errors near the 30 mÅ cutoff and imperfections in the line profiles used in the synthetic spectra, such as deficiencies in the various broadening functions used. This is unlikely to have had a major impact on the derived velocities, because the action of matching the

[5] This dependence of the line profile on χ_{low}, as well as on W, is of course important to consider when constraining the instrumental and macroturbulent broadening of other line profiles, for example those of Li and Ba, when attempting to constrain their isotopic composition.

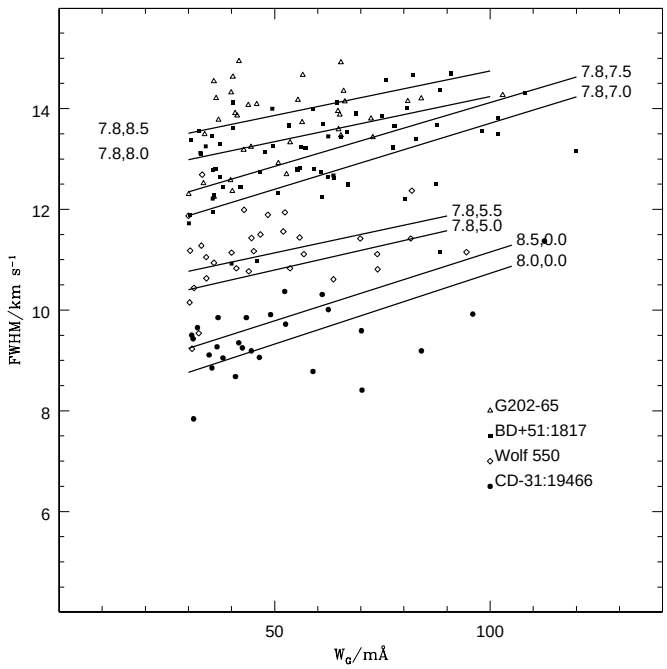

FIG. 3.—Least-squares fits to Gaussian parameters of synthetic spectra for the stated broadening velocities (in km s^{-1}). The first velocity is the FWHM of instrumental and macroturbulent origin, and the second is $v \sin i$. The observed data are also shown.

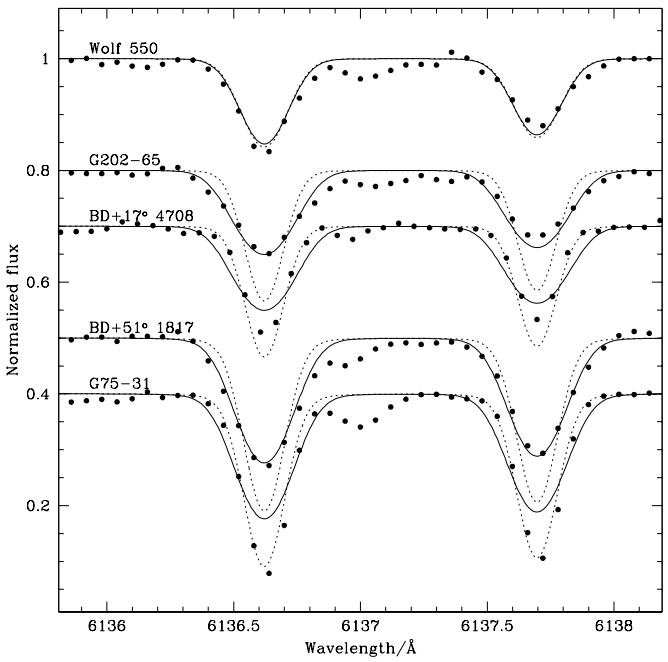

FIG. 4.—Observed and synthetic spectra of two Fe I lines for the Li-poor stars Wolf 550, G202-65, and BD +51°1817. All synthetic spectra have been broadened by a Gaussian with FWHM = 7.8 km s^{-1}, to reproduce the instrumental and macroturbulent broadening. For Wolf 550, rotational broadening with $v \sin i = 5.0$ and 5.5 km s^{-1} has been included. The two synthetic profiles are difficult to distinguish, but nevertheless have significantly different FWHM values; see Fig. 3. The synthetic spectra for G202-65 have $v \sin i = 0$ and 8.5 km s^{-1}, and those for BD +51°1817 have $v \sin i = 0$ and 7.5 km s^{-1}. These pairs of syntheses are also shown superimposed on the spectra of the Li-normal stars BD +17°4708 and G75-31, respectively.

observed and theoretical least-squares fits at a "central" value of the range of parameters (i.e., 50 mÅ) will minimize the impact of errors in the slope.

As a final illustration of the broadening, we show in Figure 4 a sample of spectra around two Fe I lines. The spectrum of Wolf 550 is overlaid by two synthetic spectra having $v \sin i = 5.0$ and 5.5 km s^{-1}. The difference between the two line profiles is very difficult to discern on any single absorption line, but Figure 3 indicates that the FWHM values are nevertheless very sensitive to this small change. It is because we have used data for a large number of Fe I lines that we have been able to achieve this level of sensitivity. Moreover, even though rotation velocities this small are challenging to measure, the key implications of this work follow from the fact that they are rotating significantly at all, rather than from the precise value of the velocity that should be assigned.

The spectrum of G202-65 in Figure 4 is also overlaid by two synthetic spectra, the deeper one having a Gaussian broadening of FWHM = 7.8 km s^{-1}, but no rotational broadening, and the shallow one having the same Gaussian broadening and $v \sin i = 8.5$ km s^{-1}. These same synthetic spectra are also overlaid on the spectrum of the Li-normal star BD +17°4708, which has line strengths similar to those of G202-65 but no discernible rotational broadening. The differences between the nonrotating and rotating profiles are clear.

A similar comparison is made in the case of BD +51°1817, where the deeper spectrum again has Gaussian broadening of FWHM = 7.8 km s^{-1} but no rotational broadening, and the shallow profile has the same Gaussian broadening and $v \sin i = 7.5$ km s^{-1}. These synthetic spectra are overlaid on the spectrum of the Li-normal star G75-31, which has line strengths similar to those of BD +51°1817 but no discernible rotational broadening. The comparison makes clear that the profiles give reasonable fits to the spectra, but we emphasize again that the greatest sensitivity comes from measuring the FWHM of a larger number of lines, as shown in Figures 2 and 3.

We note that independently, Carney et al. (2001) have assigned "marginally significant detections" of rotation velocities for these stars between 6 and 10 km s^{-1}. Their data, taken with S/N from 7 to 50 per resolution element (5–35 pixel^{-1}?), did not allow them to achieve the same precision as here, but the similarity of their "marginal" detections to the more precise results derived here verify their ability to identify the presence of rotational broadening and derive approximate rotation velocities even from low–S/N spectra.

3.3. *Metallicities*

The metallicities of the stars estimated from photometry and low-resolution spectroscopy (Ryan et al. 2001b) have been improved using the high-resolution spectra. That analysis is discussed more fully by A. Ford et al. (2002, in preparation). When the original photometric estimates of $T_{\rm eff}$ and surface gravities $\log g = 4.2$ were adopted, the calculated metallicities were in good agreement with those originally inferred. For the 18 stars in the original program, the mean difference was $\langle [{\rm Fe/H}]_{\rm new} - [{\rm Fe/H}]_{\rm old} \rangle = 0.02$ dex, with a standard deviation of 0.14 dex, consistent with the error estimates presented originally. The old and new values are listed for the Li-poor stars in columns (8) and (9), respectively, of Table 1.

3.4. *Effective Temperatures*

Calculations were also made of the effective temperatures that would be inferred for each star by nulling the dependence of derived abundance on excitation potential. For the 18 stars, $T_{\rm eff}$ increased by on average 246 K from this process, although with a broad standard deviation of 179 K. The inferred metallicities increased accordingly. However, for two of the hot Li-depleted stars, the inferred $T_{\rm eff}$ increased by more than 500 K, implying $T_{\rm eff} \sim 6900$ K. Such high temperatures would push those stars clear of the main-sequence turnoff and would greatly strengthen their association with traditional blue stragglers. If their temperatures are that high, they would almost certainly be genuine blue stragglers and their association with subturnoff-mass objects would be incorrect. However, even in that case we would have two new problems to consider: why the photometric colors of these stars would be incompatible with their effective temperatures, and how many other superturnoff-mass blue stragglers might also be masquerading as subturnoff-color stars. We note that the photometric effective temperatures derived by us (Ryan et al. 2001b) are consistent with those of Carney et al. (2001), although both are based on similar photometry.

Alternative diagnostics of the effective temperature may help resolve this problem. Two of the Li-poor stars have available 1–2 Å resolution spectroscopy, obtained during the course of the HK survey of Beers and colleagues (see Beers et al. 1999 and references therein). A calibration of $T_{\rm eff}$ based on the strength of a Balmer line index (HP2) and tied to the infrared flux method (IRFM) scale of Alonso, Arribas, & Martínez-Roger (1996) yields temperature estimates $T_{\rm eff} = 6223 \pm 125$ K for BD $+51^\circ 1817$ and $T_{\rm eff} = 6286 \pm 125$ K for Wolf 550. Furthermore, Wolf 550 (=G66-30) is one of the stars measured by Alonso et al. (1996), who report $T_{\rm eff} = 6211 \pm 107$ K. All these results are consistent with the temperatures we derived from photometric measurements, thus strengthening our belief that they, rather than the spectroscopic determinations, are appropriate. Nevertheless, the higher effective temperatures and corresponding metallicities that would be inferred from the spectral analysis are also given in Table 1 (cols. [10] and [11], respectively).

4. DISCUSSION

4.1. *Characterizing the Stars*

Besides rotation, there is one additional difference, and possibly two, between the three broadened Li-depleted stars and the one nonbroadened one. First, the three broadened stars are very close to the halo main-sequence turnoff, having 6269 K $\leq T_{\rm eff}$ (photometric) $\leq$ 6390 K, whereas CD $-31^\circ 19466$ is cooler, with $T_{\rm eff} = 5986$ K (Ryan et al. 2001a). Second, Carney et al. (1994, 2001) and D. Latham (2000, private communication) list all three of the hot group as confirmed binaries. Their periods $P_{\rm orb}$ (where only the last digit is uncertain) and eccentricities e are listed in Table 1. The binary status of the nonrotating Li-depleted star is not yet known.

As the $v \sin i$ measurements are lower limits on the equatorial rotation velocities v, we can derive upper limits on the rotation periods. The sidereal period of the Sun is 25.4 days, giving $v_\odot = 2.0$ km s^{-1}. The projected surface velocities of the rotating Li-poor stars are typically 3–4 times as high, and their zero-age main-sequence (ZAMS) radii can be estimated for inferred masses of 0.8 $M_\odot$ as $R_{\rm ZAMS} \simeq 0.8\ R_\odot$, assuming Population I structures. Halo stars, having lower opacity, will be slightly more compact than Population I stars for a given mass. On the other hand, stars at the turnoff will have larger radii than ZAMS objects, being more evolved. The ZAMS radius would lead to rotation periods of typically only 7 days; even a factor of 2 increase in radius would increase the rotation periods to only 14 days. These rotation periods are well below the current orbital periods, and hence the orbits are not currently tidally synchronized.

4.2. *Evolutionary Histories and Spin-up*

If rotation is responsible for the broadening, then one of two histories may be invoked: (1) these stars formed with unusually high rotation velocities $\simeq$14 Gyr ago and have not yet spun down; or (2) they have acquired angular momentum during their lifetimes. Option 1 is rather ad hoc; while the details of the way stars spin down are not understood completely (see, e.g., Sills, Pinsonneault, & Terndrup 2000), it is unclear how a small fraction of the halo population could avoid the spin-down that every other halo dwarf seems to have experienced. Option 2, on the other hand, could result from a range of mechanisms that are already well studied, such as mass transfer onto the star from a companion, an event that also transfers angular momentum, or spin-up in a merger. These mechanisms have already been proposed by Ryan et al. (2001a) as possibly responsible for the formation of the ultra–Li-deficient stars; that work preceded the detection of rotation.

The three rotating stars we have investigated are similar in many respects to the thick-disk, binary blue straggler HR 4657 identified by Fuhrmann & Bernkopf (1999). Fuhrmann & Bernkopf (1999) likewise drew a connection between rapid rotation, Li depletion, and mass transfer from a companion. Our present results strengthen the evidence for this connection, which we now make in three additional cases and which we explore in more detail below. We note that our sample also extends this connection from the thick disk to the halo, since the space velocities of G202-65 and Wolf 550 are indisputably those of halo stars, even if BD $+51^\circ 1817$ might be more correctly associated with the thick disk (Table 2 of Ryan et al. 2001b).

The possibility that the broadened stars acquired additional angular momentum via mass transfer seems particularly plausible-given the confirmed binary status of all three of these objects, since we can then point to a likely mass donor. Moreover, Carney et al. (2001) infer projected companion masses $M_2 \sin i < 0.55\ M_\odot$, compatible with their being the white dwarf remnants of stars initially more massive than the 0.8 $M_\odot$ normally associated with the halo main-sequence turnoff.

The current rotation velocities of the three stars are well below the high values that are *initially* obtained during mergers. Calculations by Webbink (1976) showed velocities greater than 100 km s^{-1} maintained throughout the main-sequence lifetime of a merger product, dropping only to $v_{\rm rot} = 89.4$ km s^{-1} by the time it reached the base of the giant branch. More recent work (Sills et al. 1997; Leonard & Livio 1995) raised the possibility that such objects would spin down during hydrogen burning if the merger product goes through a period of expansion and subsequent recontraction that resembles pre–main-sequence evolution, which is

when most of the spin-down of single low-mass stars occurs (Sills et al. 2000). The low velocities offer no support for an unrelaxed merger of the type studied by Webbink but cannot rule out a merger that subsequently spins down as modeled by Leonard & Livio. However, the need for a merger history is obviated by the existence of a present companion, which is an alternative angular momentum donor.

Han et al. (1995) examine four binary evolutionary channels by which matter could be transferred onto stars. Investigating Ba and CH stars, they find that mass transfer via Roche lobe overflow leads to 10^2–10^3 day periods. (They studied both stable and unstable transfer, the latter involving common envelope ejection.) On the other hand, accretion from a stellar wind ("wind accretion" and "wind exposure") leads to periods of 10^3–10^5 days. Stars that experience Roche lobe overflow are expected to circularize their orbits on a short timescale. However, Carney et al. (2001) find significantly nonzero eccentricities for two of the three binary systems, Wolf 550 and G202-65, which makes it unlikely that Roche lobe overflow occurred in these systems. If the initially more massive companion was always well inside its Roche lobe, tidal circularization would have been ineffective (see, e.g., Zahn 1977), and the observed eccentricities would effectively be primordial.

An alternative possibility is that the orbits *were* circularized in the past, but the sudden mass loss from the system in a subsequent supernova explosion caused nonzero present-day eccentricities. In this case, the invisible companion would be a neutron star, and its likely mass would be 1.4 $M_\odot$, since most measured neutron star masses sit very close to this value (see, e.g., Charles 1998). However, the measured mass functions would then imply uncomfortably small inclination angles for at least two of the three systems (see col. [15] of Table 1). As any Type II supernova explosion is likely to have ejected more than twice the current binary mass ($\simeq 2\ M_\odot$), the system could not have survived a spherically symmetric explosion in which the postsupernova orbital speed is larger than the escape speed. However, survival would be possible if the neutron star received a suitably directed kick velocity at birth. Such kicks are inferred from the observed proper motions of pulsars (see, e.g., Kalogera 1996).

A phase of Roche lobe overflow may have occurred in BD +51°1817, whose eccentricity is much lower. The present system parameters are consistent with the remnant configuration of a stable mass transfer phase with a low-mass giant donor. In that case, the companion would be a white dwarf, and the orbital period should be consistent with an approximate orbital period–white dwarf mass relation (see, e.g., Webbink, Rappaport, & Savonije 1983) that reflects the radius (R_2)–core mass (M_c) relation of low-mass giant stars. For moderate Population II metallicity $Z = 0.001$, this is

$$\frac{R_2}{R_\odot} = 10^{3.36}\left(\frac{M_c}{M_\odot}\right)^{4.17} \quad (1)$$

(see, e.g., Ritter 1999). Combining this with Kepler's third law for a semidetached system,

$$\log_{10}\frac{P_{\rm orb}}{\rm days} = 1.5\log_{10}\left(\frac{R_2}{R_\odot}\right) - 0.5\log_{10}\left(\frac{M_2}{M_\odot}\right) - 0.433\ , \quad (2)$$

we can express the orbital period of a Roche lobe–filling giant in terms of its mass and core mass. Assuming that mass transfer removes the entire envelope (so that $M_2 = M_c$) gives a white dwarf remnant mass $M_2 \simeq 0.47\ M_\odot$, consistent with the mass function measured by Carney et al. (2001). This mass would imply an orbital inclination $i \simeq 48°$.

The progenitor of BD +51°1817 could have escaped unstable mass transfer only if the initial mass ratio was not far from unity, so that the initially more massive star can shed enough mass in a wind on the AGB to become the less massive component at Roche lobe contact. This is required because convective stars, such as giants, expand upon mass loss, and only if the mass ratio $q = M_{\rm donor}/M_{\rm accretor}$ is sufficiently small can the Roche lobe expand fast enough to keep the expanding star in check. For conservative mass transfer from a fully convective star, this stability limit is $q \lesssim 2/3$ (see, e.g., Webbink 1985).

We can estimate an upper limit on the transferred mass ΔM in the phase of stable Roche lobe overflow by assuming that the evolution was conservative, i.e., it proceeded with constant binary mass and constant orbital angular momentum. In that case the product $M_1^3 M_2^3 P_{\rm orb}$ is constant throughout the evolution (M_1 is the accretor mass). If the mass ratio *at the beginning of Roche lobe overflow* was close to the critical value 2/3, the current masses ($M_1 = 0.90\ M_\odot$, $M_2 = 0.47\ M_\odot$) then imply initial masses $M_{1,i} = 0.82\ M_\odot$, $M_{2,i} = 0.55\ M_\odot$, i.e., $\Delta M \lesssim 0.08\ M_\odot$. (Of course, the donor would have been even more massive during its main-sequence lifetime, before nonconservative mass loss via winds set in.)

If, on the other hand, the mass ratio at Roche lobe contact was larger than the critical value, the progenitor of BD +51°1817 would have experienced dynamically unstable mass transfer from a giant star, leading to a short-lived common envelope phase. The orbit tightens as orbital energy is used to eject the envelope of the giant star (see, e.g., Iben & Livio 1993 for a review). In this scenario, the fact that the post–common envelope orbit is still fairly wide implies that the binding energy of the giant immediately before Roche lobe contact was small.

Given these possibilities for the evolutionary history, the three Li-depleted halo stars could have accreted mass and thus acquired angular momentum. The circular orbit of BD +51°1817 allows this to have occurred during Roche lobe overflow or a common envelope phase, whereas the other stars with nonzero eccentricities are more compatible with accretion from a stellar wind.

Although it is clear that the stars are not tidally synchronized in their *present* orbits, we briefly considered the possibility that the rapid spin of these binary components could be left over from earlier tidal synchronization, when the orbital separation was much less. This would require that the stars once had orbital periods as short as 7–14 days, were synchronized at that time, and subsequently migrated apart. Clearly, this is not possible for BD +51°1817 if the companion is a white dwarf. If there was stable Roche lobe overflow, the initial orbital period must have been longer than 400 days; if there was a common envelope phase, the initial period must have been even longer than the current period. Wind losses could have increased the orbital period, but not by such a large factor. If the angular momentum per unit mass in the wind is the specific orbital angular momentum of the corresponding star, the orbital period increases as $P_{\rm orb} \propto 1/M^2$ (where M is the total binary mass). Hence, to

increase the binary period from 14 days to the current values, the total binary mass must have decreased by a factor between 3 and 7, i.e., by more than $\simeq 5\ M_\odot$. Stars are thought to lose that much mass only in the late stages of their evolution when they are large—too large to fit inside the small orbit that corresponds to $P_{\rm orb} = 14$ days. If, on the other hand, the present companion of any of the three systems considered here is a neutron star, then the orbital period could have been as short as 14 days, after a common envelope phase that removed the hydrogen envelope of the progenitor of the neutron star. However, such a tight system would then not be able to increase its orbital separation through the supernova, as even in the presence of kick velocities the orbital separation cannot increase by more than a factor of 2 (Kalogera 1996). We conclude that none of the three systems discussed here ever had an orbital period as short as 14 days.

4.3. *Mass and Angular Momentum Estimates*

4.3.1. *Roche Lobe Overflow*

In the case of Roche lobe overflow, an accretion disk would form, since the circularization radius is typically a tenth of the orbital separation and hence larger than the likely stellar radius of the accretor in most cases. If the Keplerian disk extends down to the surface of the accretor, the disk material carries the angular momentum per unit mass, j, given by

$$j = \sqrt{GM_1R_1}\ , \tag{3}$$

where M_1 and R_1 are the mass and radius of the accretor, respectively. Then the gain of angular momentum, ΔJ, is

$$\Delta J = \int \dot{M}_1 j\, dt = \int j\, dM_1\ . \tag{4}$$

Assuming a simple main-sequence mass-radius relation

$$\frac{R_1}{R_\odot} = r_0 \frac{M_1}{M_\odot} \tag{5}$$

(where $r_0 \simeq 1$), this becomes

$$\Delta J = \frac{1}{2}\sqrt{\frac{GR_1}{M_1}}\left(M_1^2 - M_{1,i}^2\right), \tag{6}$$

where $M_{1,i}$ is the initial accretor mass. Writing the accretor's moment of inertia as $k^2 M_1 R_1^2$ (where $k^2 \simeq 0.1$) and assuming that the initial spin is zero gives

$$\frac{M_{1,i}}{M_1} = \left(1 - 2k^2\frac{P_k}{P}\right)^{1/2}\ , \tag{7}$$

where P is the current spin period and P_k the "break-up" spin period,

$$P_k = \frac{2\pi}{\sqrt{GM_1/R_1^3}} \simeq 0.1 \text{ days}\ . \tag{8}$$

Equation (7) shows that the accretion of only $\Delta M = M_1 - M_{1,i} \simeq 10^{-3}\ M_\odot$ spins up the accretor to rates comparable to the currently observed spin period $P \simeq 7$ days. If the rapid rotation is restricted to the convective envelope of the accretor, the required accreted mass is only $\simeq 10^{-4}\ M_\odot$ (with $k^2 \simeq 0.01$ in the expression for the moment of inertia, from, e.g., our own Population II stellar models, calculated with Mazzitelli's stellar code; Mazzitelli 1989).

As we measure only the projected velocity $v \sin i$, the actual velocities may be greater; the periods may then be shorter than $P \simeq 7$ days. If the period were only $P \simeq 1$–2 days, as would also be the case if the companion is a neutron star at low inclination (see Table 1), we would infer $\Delta M = 10^{-2}\ M_\odot$.

It is clear from these analyses that accretion of quite small masses would be sufficient to spin up these objects.

4.3.2. *Slow-Wind Accretion*

In the case of accretion from a sufficiently slow wind of a companion that is not too far from its Roche lobe, an accretion disk may still form, so that the same estimate for ΔJ and ΔM applies.

4.3.3. *Fast-Wind Accretion*

In the case of a fast wind, the accretion flow can be described as Bondi-Hoyle accretion. Here the specific angular momentum j of the accreted material is difficult to estimate; three-dimensional hydrodynamical simulations (Ruffert 1999) show that j is a fraction $f \simeq 0$–0.7 of the total angular momentum per unit mass available in the accretion cylinder. If the accretion radius is of order the stellar radius, this translates into a relation similar to equation (7), but with a coefficient $\simeq k^2/f$ instead of k^2. So, for example, if $f = 0.1$, the accreted mass would have to be $\Delta M \simeq 10^{-2}\ M_\odot$. Given the small capture efficiency and short lifetime of phases with large wind-loss rates, the total wind-accreted mass is typically $\lesssim 0.1\ M_\odot$, which is adequate, but might be much smaller (see, e.g., King & Kolb 1999).

4.3.4. *Common Envelope Phase*

In the case of a common envelope phase, the net mass gain is probably small, perhaps $\lesssim 10^{-2}$–$0.1\ M_\odot$ (Hjellming & Taam 1991). The specific angular momentum of the accreted material is presumably similar to that of the Bondi-Hoyle case.

4.3.5. *Caveats*

The calculations above assume that the stars have not spun down significantly following the mass transfer event. If the currently observed spin is due to an episode of mass accretion several Gyr ago, it is likely that the stars have spun down significantly via magnetic stellar wind braking. Hence, our estimates for the accreted mass must be seen as lower limits.

4.4. Li *Depletion in a Mass Transfer Binary*

The link between Li depletion and rapid rotation is easy to envisage in a mass transfer scenario. Revisiting discussions by Norris et al. (1997) and Ryan et al. (2001a), at least three possibilities exist if the rapid rotation reflects angular momentum transfer onto the turnoff star via mass accretion. (1) Triggered mixing: depending on how the surface of the accretor is disturbed by the accreting plasma, additional mixing may be induced that carries the surface Li to depths where it is destroyed. (2) Prior destruction: even if no substantial mixing was triggered in the accretion event, both stars may have been devoid of Li already once mass transfer began. In this scenario, the donor would destroy its original

Li during its giant branch evolution (or earlier), and/or the accretor may have initially been of sufficiently low mass ($M \lesssim 0.7\ M_{\odot}$) that it too had already destroyed its Li by conventional means. (3) Accretion-dominated surface: if the mass accreted is higher than the mass of the accretor's surface convection zone, then the composition of the material now observed may reflect solely that of the donor, which had already destroyed its Li, as in scenario 2. Estimates by Norris et al. (1997; their Fig. 3) show that only a few times $10^{-2}\ M_{\odot}$ of Li-free material need be accreted to produce a Li-free surface convective zone. This quantity is compatible with the mass ranges estimated above.

4.5. *The Nonrotating* Li-*poor Star*

Although this explanation may work for the three line-broadened stars, how should we interpret the unbroadened one? It is, of course, possible that this star is rotating rapidly, but with a low inclination i that renders it unobservable. The same explanation could account for the lack of evidence of radial velocity variations, since the angular momentum acquired during the accretion process would be aligned with the orbital angular momentum. Detection of a companion to the fourth star would provide support for our hypothesis. However, in view of the temperature differences between the hottest three and the unbroadened fourth, we echo the warning of Ryan et al. (2001a) that more than one explanation may be required for the formation of the ultra–Li-depleted stars. It is clearly important to continue the investigation of the remaining sample of ultra–Li-depleted objects to determine whether or not they have a common origin. The chemical signatures of this class of stars, already explored initially by Norris et al. (1997) and Ryan et al. (1998), will be pursued elsewhere (A. Ford et al. 2002, in preparation).

4.6. *Constraints on* Li *Processing in Single Stars*

Most single halo stars have spun down to extremely low velocities over their long histories, so the existence of high rotation in such old stars requires that a torque has been exerted on them by some means. Mass transfer is one of the most effective ways of achieving this. The compelling evidence for mass transfer having occurred in three of the four Li-depleted stars in our sample emphasizes that these stars can tell us nothing about the primordial Li abundance. If cooler examples of Li-depleted stars (distributed over the range of temperatures encompassing the Spite plateau) are also found to exhibit evidence of past mass transfer episodes that might be responsible for the destruction of their surface Li, it becomes clear that such objects cannot be viewed as the high-depletion tail of the same processes that are invoked to account for the long-term evolution of surface Li abundances in single stars (see, e.g., Pinsonneault et al. 2002). In that case, efforts to study the way single stars destroy Li as they age will have to avoid incorporating such objects in their samples.

5. SUMMARY AND CONCLUDING REMARKS

The discovery of line broadening and its likely origin in the rapid rotation of three of the four ultra–Li-depleted stars strongly suggests that these stars have acquired angular momentum from a companion star. This possibility is made more plausible by the observation that all three are single-lined spectroscopic binaries with lower mass companions. The angular momentum transfer will have been effected by mass transfer, by stable Roche lobe overflow, or by a common envelope phase, in the case of the circularized system, or wind accretion, for the eccentric systems. Estimates of the specific angular momentum of accreted material indicate that quite small transfer masses could have been involved, although the unknown subsequent spin-down of the accretor prevents us from assigning definitive values for each star. In these cases the Li deficiency could be explained in three ways: (1) mixing induced by the accretion event, (2) prior destruction, where both stars may have been devoid of Li already when mass transfer began, and (3) the likelihood that we now observe a surface dominated by accreted material, which reflects the surface composition of the donor, which had destroyed its own Li prior to the mass transfer event.

These findings add weight to the suggestion of Ryan et al. (2001a) that the ultra–Li-depleted stars, or at least the hottest subset of them, may be subturnoff-mass counterparts of traditional field blue stragglers. Although binarity alone does not provide evidence of mass transfer, high angular momentum in systems too wide to be tidally synchronized does.

The authors thank the UK Panel for the Allocation of Telescope Time (PATT) and the Director and staff of the Anglo-Australian Telescope (AAT) and William Herschel Telescope (WHT) for the provision of research facilities. S. G. R. was supported by PPARC grant PPA/O/S/1998/00658. T. C. B. acknowledges partial support from NSF grants AST 00-98549 and AST 00-98508. U. C. K. acknowledges partial support from PPARC grant PPA/G/S/1999/00127.

REFERENCES

Alonso, A., Arribas, S., & Martínez-Roger, C. 1996, A&AS, 117, 227
Beers, T. C., Rossi, S., Norris, J. E., Ryan, S. G., & Shefler, T. 1999, AJ, 117, 981
Carney, B. W., Latham, D. W., Laird, J. B., & Aguilar, L. A. 1994, AJ, 107, 2240
Carney, B. W., Latham, D. W., Laird, J. B., Grant, C. E, & Morse, J. A. 2001, AJ, 122, 3419
Cayrel, R., Lebreton, Y., & Morel, P. 1999, Ap&SS, 265, 87
Charles, P. 1998, in Theory of Black Hole Accretion Disks, ed. M. Abramowicz, G. Bjornsson, & J. E. Pringle (Cambridge: Cambridge Univ. Press), 1
Cottrell, P. L., & Norris, J. 1978, ApJ, 221, 893
Ferraro, F. R., Fusi Pecci, F., & Bellazzini, M. 1995, A&A, 294, 80
Fuhrmann, K., & Bernkopf, J. 1999, A&A, 347, 897
Gray, D. F. 1992, The Observation and Analysis of Stellar Photospheres (Cambridge: Cambridge Univ. Press)
Han, Z., Eggleton, P. P., Podsiadlowski, P., & Tout, C. A. 1995, MNRAS, 277, 1443
Hjellming, M. S., & Taam, R. E. 1991, ApJ, 370, 709
Hobbs, L. M., & Mathieu, R. D. 1991, PASP, 103, 431
Hobbs, L. M., Welty, D. E., & Thorburn, J. A. 1991, ApJ, 373, L47
Iben, I., Jr., & Livio, M. 1993, PASP, 105, 1373
Kalogera, V. 1996, ApJ, 471, 352
King, A. R., & Kolb, U. 1999, MNRAS, 305, 654
Lambert, D. L., Heath, J. E., & Edvardsson, B. 1991, MNRAS, 253, 610
Leonard, P. J. T., & Livio, M. 1995, ApJ, 447, L121
Mateo, M., Harris, H. C., Nemec, J., & Olszewski, E. W. 1990, AJ, 100, 469
Mazzitelli, I. 1989, ApJ, 340, 249
Nissen, P. E., Asplund, M., Hill, V., & D'Odorico, S. 2000, A&A, 357, L49
Nissen, P. E., Lambert, D. L., & Smith, V. V. 1994, Messenger, 76, 36
Norris, J. E., Ryan, S. G., Beers, T. C., & Deliyannis, C. P. 1997, ApJ, 485, 370

Pilachowski, C. A., Sneden, C., & Booth, J. 1993, ApJ, 407, 699
Pinsonneault, M. H., Steigman, G., Walker, T. P., & Narayanan, V. K. 2002, ApJ, in press
Preston, G. W., & Sneden, C. 2000, AJ, 120, 1014
Ritter, H. 1999, MNRAS, 309, 360
Romano, D., Matteucci, F., Molaro, P., & Bonifacio, P. 1999, A&A, 352, 117
Ruffert, M. 1999, A&A, 346, 861
Ryan, S. G., Beers, T. C., Kajino, T., & Rosolankova, K. 2001a, ApJ, 547, 231
Ryan, S. G., Beers, T. C., Olive, K. A., Fields, B. D., & Norris, J. E. 2000, ApJ, 530, L57
Ryan, S. G., & Deliyannis, C. P. 1995, ApJ, 453, 819
———. 1998, ApJ, 500, 398
Ryan, S. G., Kajino, T., Beers, T. C., Suzuki, T. K., Romano, D., Matteucci, F., & Rosolankova, K. 2001b, ApJ, 549, 55
Ryan, S. G., Norris, J. E., & Beers, T. C. 1998, ApJ, 506, 892
———. 1999, ApJ, 523, 654
Sills, A., Lombardi, J. C., Jr., Bailyn, C. D., Demarque, P., Rasio, F. A., & Shapiro, S. L. 1997, ApJ, 487, 290
Sills, A., Pinsonneault, M. H., & Terndrup, D. M. 2000, ApJ, 534, 335
Smith, V. V., Lambert, D. L., & Nissen, P. E. 1998, ApJ, 506, 405
Spite, F., & Spite, M. 1982, A&A, 115, 357
Spite, M., Maillard, J. P., & Spite, F. 1984, A&A, 141, 56
Spite, M., Molaro, P., François, P., & Spite, F. 1993, A&A, 271, L1
Thorburn, J. A. 1992, ApJ, 399, L83
———. 1994, ApJ, 421, 318
Webbink, R. F. 1976, ApJ, 209, 829
———. 1985, in Interacting Binary Stars, ed. J. E. Pringle & R. A. Wade (Cambridge: Cambridge Univ. Press), 39
Webbink R. F., Rappaport, S., & Savonije, G. J. 1983, ApJ, 270, 678
Zahn, J.-P. 1977, A&A, 57, 383